PEACH: Proactive and Environment-Aware Channel State Information Prediction with Depth Images

SERKUT AYVAŞIK, Chair of Communication Networks, Technical University of Munich, Germany
FIDAN MEHMETI, Chair of Communication Networks, Technical University of Munich, Germany
EDWIN BABAIANS, Chair of Media Technology, Technical University of Munich, Germany
WOLFGANG KELLERER, Chair of Communication Networks, Technical University of Munich, Germany

Up-to-date and accurate prediction of Channel State Information (CSI) is of paramount importance in Ultra-Reliable Low-Latency Communications (URLLC), specifically in dynamic environments where unpredictable mobility is inherent. CSI can be meticulously tracked by means of frequent pilot transmissions, which on the downside lead to an increase in metadata (overhead signaling) and latency, which are both detrimental for URLLC. To overcome these issues, in this paper, we take a fundamentally different approach and propose PEACH, a machine learning system which utilizes environmental information with depth images to predict CSI amplitude in beyond 5G systems, without requiring metadata radio resources, such as pilot overheads or any feedback mechanism. PEACH exploits depth images by employing a convolutional neural network to predict the current and the next 100 ms CSI amplitudes. The proposed system is experimentally validated with extensive measurements conducted in an indoor environment, involving two static receivers and two transmitters, one of which is placed on top of a mobile robot. We prove that environmental information can be instrumental towards proactive CSI amplitude acquisition of both static and mobile users on base stations, while providing an almost similar performance as pilot-based methods, and completely avoiding the dependency on feedback and pilot transmission for both downlink and uplink CSI information. Furthermore, compared to demodulation reference signal based traditional pilot estimation in ideal conditions without interference, our experimental results show that PEACH yields the same performance in terms of average bit error rate when channel conditions are poor (using low order modulation), while not being much worse when using higher modulation orders, like 16-QAM or 64-QAM. More importantly, in the realistic cases with interference taken into account, our experiments demonstrate considerable improvements introduced by PEACH in terms of normalized mean square error of CSI amplitude estimation, up to 6 dB, when compared to traditional approaches.

CCS Concepts: • **Computing methodologies** → **Neural networks**; • **Networks** → **Network measurement**; **Network experimentation**; **Mobile networks**; **Network reliability**.

Additional Key Words and Phrases: 5G New Radio; URLLC; Measurement; Dataset; Environment-Aware Wireless Communications; Wireless Channel Estimation; Channel State Information; Proactive Prediction; Convolutional Neural Network

ACM Reference Format:
Serkut Ayvaşık, Fidan Mehmeti, Edwin Babaians, and Wolfgang Kellerer. 2023. PEACH: Proactive and Environment-Aware Channel State Information Prediction with Depth Images. *Proc. ACM Meas. Anal. Comput. Syst.* 7, 1, Article 24 (March 2023), 27 pages. https://doi.org/10.1145/3579450

Authors' addresses: Serkut Ayvaşık, serkut.ayvasik@tum.de, Chair of Communication Networks, Technical University of Munich, Germany; Fidan Mehmeti, fidan.mehmeti@tum.de, Chair of Communication Networks, Technical University of Munich, Germany; Edwin Babaians, edwin.babaians@tum.de, Chair of Media Technology, Technical University of Munich, Germany; Wolfgang Kellerer, wolfgang.kellerer@tum.de, Chair of Communication Networks, Technical University of Munich, Germany.

2476-1249/2023/3-ART24
https://doi.org/10.1145/3579450

1 INTRODUCTION

Ultra-Reliable Low-Latency Communications (URLLC) are one of the three service types supported in 5G networks [25]. These services are characterized by very stringent traffic requirements to deliver within a very short time (on the order of milliseconds) the vast majority of the packets. Autonomous driving, remote surgery, remote monitoring and control, and industrial automation in general [57] are some use cases that belong to services with URLLC traffic. The aforementioned services are not only sensitive to abiding by those very non-flexible requirements, but also, because of their nature, a failure to comply either with the low-latency or reliability requirement can give rise to a serious risk on human lives. Therefore, the paramount importance of enabling (almost) flawless operation of this type of traffic.

Although 5G networks are being deployed since recently, its shortcomings are already recognized around enabling URLLC traffic [41, 56]. Moreover, beyond 5G/6G wireless systems are envisioned to pave the road further for industrial automation with even more stringent latency (decreased even more down to 1 ms) and reliability (to almost 100%) requirements [22, 58], especially for mission-critical communications [24, 46]. This will be very strenuous to the successful operation of wireless networks.

The fundamental problem of URLLC is to satisfy the strict requirements of reliability and latency simultaneously. The enhancement of the reliability depends heavily on accurate channel estimation to mitigate wireless channel distortion, which requires channel probing. On the other hand, the reduction of latency requires lower processing times and less signaling. Given that these two requirements are conflicting, accurate channel estimation (metadata increases) and channel information feedback (latency increases) for the URLLC are one of the main challenges [25]. Predicting fading wireless channels correctly is of high importance for a reliable communication and is still very challenging [29]. While the standardization for 5G targeted latency reduction via new subcarrier spacing (SCS) structure to have shorter slot duration and allowing shorter transmission time intervals (TTIs), the signaling overhead for control messages was initially neglected. However, especially for URLLC where short-packet sizes are expected [1], the metadata such as channel estimation feedback, pilot transmissions or grant-based random access procedures have to be taken into account [20, 25, 57]. Resource allocation along with grant-based scheduling request hinders the URLLC systems to have at most one retransmission because of the latency restriction [48]. State-of-the-art solutions propose grant-free (GF) access schemes in the uplink (UL) in order to reduce the latency further in the current 5G systems [18, 38]. The GF access is foreseen to eliminate the large latency and signaling overhead existing in grant-based schemes for the conventional random access procedures [17]. Although the current 5G New Radio (5G NR) includes GF as potential access scheme for URLLC [2], the latency reduction from GF comes with the trade-off of having more collisions due to uncontrolled access, requiring reliability improvements by means of alternative techniques such as successive interference cancellation (SIC) or increased power for URLLC user [38, 50] that do not depend on retransmissions. However, practical SIC usage depends on recent wireless channel knowledge of colliding users and the power increase for URLLC is not fair for the users with other types of services, and is not scalable.

While the signaling component in 5G is much more flexible and reduced compared to LTE, there is still a considerable signaling part required to enable URLLC services in 5G, mainly due to channel estimation [41, 46, 47]. The metadata for channel estimation is not negligible when considering the short-packet transmission in URLLC, where a higher overhead in terms of resources results in more accurate channel estimation; thus, it yields a better reliability while leaving less resources for the actual data which is already limited in the URLLC case [57]. For instance, for bad channel conditions where it is vital for URLLC services to be still operating reliably, the metadata-data

ratio is observed to be increasing up to 61% [47]. Moreover, channel estimation metadata, namely demodulation reference signal (DMRS), is only capable of providing channel knowledge on the used bandwidth. However, for channel dependent scheduling or link adaptation, base stations require channel sounding where the sounding reference signal (SRS) is used. Since SRS is transmitted on a wider bandwidth, it imposes higher energy consumption on the user side and also results in larger radio overhead.

Along with the above UL concerns, there are several issues on the downlink (DL) as well. The problem of obtaining DL CSI by network operators is well known in frequency-division duplex (FDD) due to the lack of reciprocity with UL CSI [12]. Therefore, FDD systems require a CSI feedback mechanism which consumes too much UL spectrum resource [37]. The same channel sounding concern also applies to DL resource allocation, in terms of link adaptation and scheduling, for which the CSI reference signal (CSI-RS) is used in a similar manner. CSI-RS also requires users to consume more energy when communicating on a wider bandwidth. Further, the information obtained via CSI-RS needs to be reported back to base stations. However, imperfect CSI caused by outdated CSI knowledge was shown to be affecting the performance significantly [49]. Similar degradation in CSI knowledge might originate from feedback delay or erroneous user CSI estimation.

In order to ensure proper functioning of URLLC in the next-generation wireless communications, Machine Learning (ML) approaches are considered to be one of the key enablers for overcoming those concerns. Considering the above-mentioned challenges, researchers were oriented to use various ML approaches to tackle fundamental limitations in URLLC for 5G/6G wireless networks [41, 46, 56], which also constitutes the basis of our work. Further, recent works on beyond 5G communication [24, 41, 46] claim that the stochastic channel models to verify the techniques/algorithms on cases such as URLLC are no longer valid since the stochastic channel models fail to model rare events for specific environments. Hence, it is advised to work on specific radio environment data and to provide proactive decision making to enable URLLC.

There are several important questions, both from research and practical perspective, which arise related to correct prediction of channel conditions while reducing metadata in wireless systems using machine learning: (1) How to provide correct CSI to base stations without or with few metadata on both UL and DL? (2) How to make intelligent scheduling and link adaptation without channel sounding? (3) How to incorporate environment-specific information towards proactive decision making in radio resource management (RRM)?

To answer these questions, in this paper, we address CSI amplitude acquisition without any pilot or feedback mechanisms with look-ahead capability and environmental awareness. We build a system for **Proactive and Environment-Aware CHannel state information prediction (PEACH)**, where depth images are used to provide CSI amplitudes for the current moment and 100 ms into the future. PEACH leverages a convolutional neural network (CNN) to map depth images of the communication environment to CSI amplitudes. The proposed system is implemented and evaluated a proof of concept of the PEACH approach on real data obtained from extensive measurements over SDRs in an indoor environment, with mobile robot and robotic arms, for multiple receivers and multiple transmitters while one transmitter is being the mobile robot itself. A typical scenario for such indoor setting would be an industrial factory floor. The performance of PEACH is compared with the traditional DMRS-based methods. PEACH is able to maintain same bit error rate (BER) performance in bad channel conditions with more conservative modulation schemes such as QPSK, while not sacrificing too much on higher modulations in an ideal communication scenario without interference. The system is also tested in a more realistic scenario with interference, where the experimental results exposed a clear advantage of PEACH in terms of better normalized mean squared error (NMSE) performance compared to DMRS (of up to 6 dB). The proposed solution provides knowledge on the entire bandwidth, which makes channel sounding obsolete, and thus the

SRS usage on UL or CSI-RS usage in DL can be avoided. Further, PEACH provides CSI knowledge into the future, where knowing the channel reliably or having CQI knowledge for the next transmissions was already shown to benefit the scheduling policies [26, 45].

Specifically, our main contributions in this work are:

- We propose a system solution for channel estimation based on video images that reliably reduces the latency for radio resource management and does not require additional metadata.
- We design and evaluate an ML framework that elucidates how to benefit from environmental awareness in wireless communications towards proactive and intelligent RRM.
- To the best of our knowledge, this is the first work that demonstrates the prediction with a high accuracy of per-subcarrier CSI amplitude in OFDM systems, specifically in 5G NR, for multiple receivers and multiple transmitters (including mobile transmitters) by using only camera images.
- To the best of our knowledge, this is also the first public 5G dataset with real wireless raw signals (I/Q samples) obtained over software defined radios (SDRs). For future research, raw wireless 5G datasets along with the camera videos are publicly available in [10].

The remainder of this work is organized as follows. In Section 2, we provide some background on the topic. This is followed by the description of the measurement setup in Section 3. Section 4 describes in detail our system, whereas some performance evaluation results with additional engineering insights are provided in Section 5. Next, in Section 6, a detailed discussion on expected and non-expected results, together with the reasons is given. Section 7 discusses some related work. Finally, Section 8 concludes the paper.

2 BACKGROUND

In this section, we provide a brief overview on channel estimation in OFDM systems and DMRS structure in 5G NR to facilitate the understanding of the remainder of this paper.

2.1 Channel Estimation

In this work, we applied common data-aided channel estimation with simple Least-Squares (LS) estimation in frequency domain for CSI acquisition from measurements with OFDM signals, specifically 5G NR signals. LS estimation is widely utilized to get initial estimates on OFDM channels with very low complexity[1]. In order to apply such a technique, the receiver must have reference information. These references are known as *training symbols* if the entire OFDM symbol consists of known signals, or *pilots* if only a couple of subcarriers in the OFDM symbol are known signals. The use of both training and pilot symbols is widely adopted depending on the reference signal structure of the communication standard. Considering a pilot-based channel estimation in frequency domain, the channel estimates are acquired over the pilot tones from

$$\hat{H}_{LS,k} = \frac{Y_k}{X_k}, \tag{1}$$

where $\hat{H}_{LS,k}$ refers to LS estimation of the channel, Y_k denotes the received signal, whereas X_k the transmitted signal at subcarrier index k. For further details on channel estimation in OFDM, readers are referred to the extensive overview in [43], and on the interpolation of pilot estimation over the frequency-time grid with different pilot tone arrangements to [15].

[1]Later, estimations are used with more complex methods to improve performance since LS estimation does not use any channel statistic knowledge among subcarriers. However, more complex methods are beyond the scope of this work as we have reference pilots for all subcarriers throughout the measurements already.

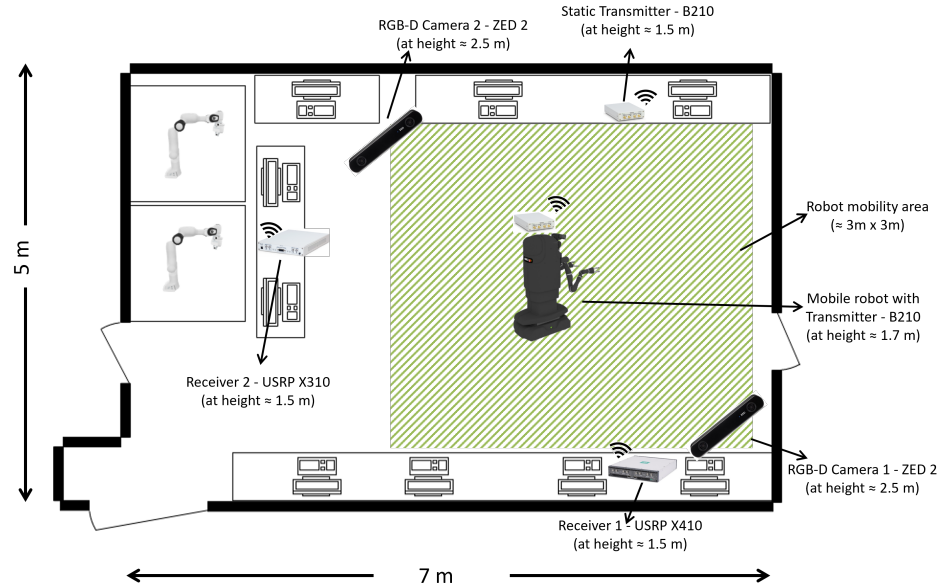

Fig. 1. The illustration of the measurement setup.

2.2 DMRS in 5G NR

The pilots in 5G NR which are used for coherent demodulation are called DMRS, similar as in LTE. 5G NR enabled flexibility on these pilot tones by allowing various location and length options as well as changing its mapping type. There are plenty of different options for the configuration of DMRS in 5G, which can be found in [4]. In this work, we have used the DMRS configuration with a length of 1 OFDM symbol, mapping type A, and configuration type 2.

3 MEASUREMENT SETUP AND IMPLEMENTATION

In this section, we first describe the environment in which the measurements were conducted as well the hardware that was used. This is followed by the description of the autonomous mobile robot system and the data acquisition process.

3.1 Measurement Environment and Hardware

The measurements were conducted in an indoor environment where there were various objects consisting of multiple robotic arms, PCs, and a mobile robot. The presence of these objects leads to a large number of multipath components in the wireless channel. A detailed representation of the environment with all objects, including the measurement equipment, along with the corresponding dimensions is depicted in Fig. 1. Such scenario represents a typical 5G setting in an industrial factory floor, for example, where static and mobile objects communicate in an indoor 5G campus network.

RGB-D cameras are selected as the Stereolabs ZED-2 stereo cameras. Both ZED-2 cameras operate by default with 60 frames per second (fps) at the resolution mode of 720p. A higher fps, i.e., 100 fps, is available at ZED-2 cameras but only with WVGA resolution. We observed that the resulting depth images from 100 fps at WVGA mode are highly fluctuating. This, in turn, could hinder the

CNN training. Another drawback of using higher resolutions, such as 1080p, is that they operate up to 30 fps, which could reduce our time resolution and diminish the effectiveness of PEACH.

SDRs for the transmitters and receivers are selected from Ettus Universal Software Radio Peripheral (USRP) SDR platforms. USRP B210s are selected for both transmitters regarding compact design and USB powered capability.[2] As receivers are selected USRP X410 and USRP X310, denoted as Rx1 and Rx2, respectively, in the remainder of this paper. The reason for selecting different receivers was to test the effect and to provide data over both SDRs, which are not easily accessible due to high cost, whereas the selection of same devices for the transmitters is to ensure equal conditions for static and mobile users named as static tx and mobile tx, respectively. USRP X410 is used with the default ZBX daughterboard and USRP X310 is used with the CBX-120 daughterboard. All SDRs are equipped with an omnidirectional antenna.

3.2 Autonomous Mobile Robot System

In our experiments, we use the Kinova®MOVO robot, an industrial dual-arm robot. It is a mobile lightweight robot with a holonomic base, designed for a multitude of research fields. The MOVO robot comes with front and rear ground-height linear 2D Light Detection And Ranging (LiDAR) sensors attached to its base. The sensor's operating frequency is 10 Hz. LiDAR is mainly used to build a sophisticated map of the environment. It is also used for 3D map and point cloud generation as well as in object detection fields. As a result of combining the data from both the front and rear LiDAR, we were able to provide autonomous navigation based on the 360° scan data. The autonomous navigation module consists of three major parts. Localization with mapping is the first part, planning is the second part, and control is the third.

For localization, we are relying on a LiDAR-based Hector slam [32] system, which is an odometer-free system to estimate robot's position and rotation in two dimensions via SLAM (Simultaneous Localization and Mapping). Hector SLAM is a relative localization method which needs to start the robot every time from the same origin. Hector SLAM is based on the optimization of the alignment of beam endpoints with the learned map. It uses the Gauss-Newton approach [33]. As a result, it is fast by not requiring a data association search between beam endpoints or an exhaustive pose search. As scans get aligned with the existing map, the matching is implicitly performed with all previous scans. We use the A-star algorithm [16] and cost-map technique from ROS navigation stack to avoid obstacles [68]. Our planner always considers the robot footprint, generates cost maps around obstacles, and provides the shortest path using the A-star algorithm.

A geometric path planning approach [59] was used to reduce the final goal reaching error of the robot. Our planned navigation path was divided into several sub-trajectories of 25 cm each. The robot rotates to the first sub-goal before navigating there. Based on the weight of reaching the next sub-goal, we control the robot's rotation during navigation. In order to keep the robot on its local trajectory and achieve the final goal, a Proportional Integral Derivative (PID) controller is used. With the setup, we achieved an average goal tracking error of 0.04 m and 15 degrees in rotation. During the operation of the robot, the maximum linear velocity was measured to be 0.15 m/s. Due to the fact that robot sensors are operating at 10 Hz, an increase in robot locomotion speed will lead to a scan matching error. Fig. 2 gives an overview of the navigation system.

Despite the fact that the navigation accuracy in real-life scenarios is satisfactory, we still have non-deterministic behaviour between the measurement runs even applying the same mobility pattern. The behavior visualization can be seen in Fig. 18 in Appendix A. This is because of the PID controllers deadband thresholds as well as the non-deterministic nature of the holonomic wheels. Due to these accumulative and non-avoidable errors, we see continuous beacon-based or tag-based

[2]In order to mount and power the SDR on the mobile robot platform, which was crucial for the operability.

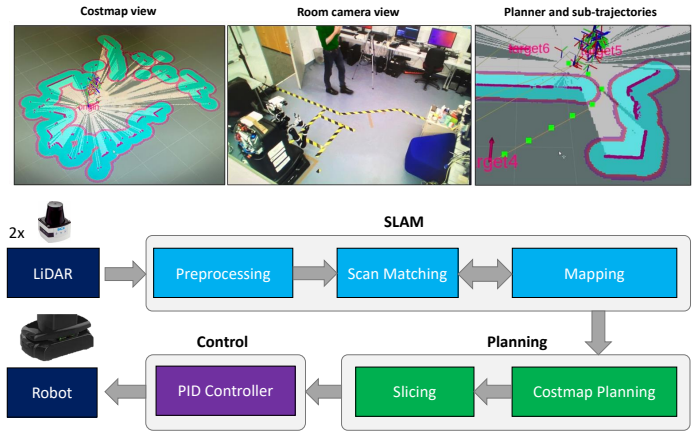

Fig. 2. An overview of the autonomous navigation system.

corrections in industrial applications. However, we do not have correction of non-deterministic errors during the measurement runs in order not to introduce additional processing delay which could affect the measurements by resulting in varying transmission intervals on the mobile robot.

3.3 Data acquisition

To provide timestamps and synchronization, a modified ZED SDK [60] is used to operate the cameras during measurements. Open-source USRP Hardware Driver (UHD) [11] code is utilized for continuous transmission and reception. The USRP gains are identical for both transmitters, but differ between receivers because they have different gain ranges. The receiving code is used as provided in raw recording to file mode; however, the transmit code is updated for synchronization and to have timestamps for each transmission. Transmissions and receptions are performed in 5G NR **band n78**, specifically at 3.74 GHz over 20 MHz bandwidth with a sampling rate of 30.72 MHz.

The programming language Matlab is used to create the 5G NR compliant waveforms for the measurements. The waveform is at length of 10 ms, namely one radio frame. The waveform includes a synchronization signal block (SSB), 30 kHz and 15 kHz SCS, with QPSK, 16-QAM and 64-QAM modulation types on different slots. SSB is used at the initial slot with 30 kHz SCS for frequency offset estimation. The assigned modulation and coding rates used in the waveform are taken from the 3GPP standard [3]. The waveform structure is displayed in Fig. 3. As illustrated in Fig. 3, in total 15 different PDSCH configurations are included in the waveform. The details regarding these configurations such as Modulation and Coding Scheme (MCS) index, modulation, target code rate and spectral efficiency are provided in Table 1. A DMRS configuration with a length of 1 OFDM symbol, mapping type A and configuration type 2 is used for each slot. To ease the comparison, only the results pertaining to 30 kHz SCS are considered.

A real-time clock synchronization between the hosts is required for the measurement setup so that the timestamps from each device are aligned for mapping the image instances to the correct transmissions. In our setup, we utilize the network time protocol (NTP) to perform the synchronization. We use our measurement-dedicated Wi-Fi connection on the robot for synchronization purposes and all the other hosts, including the NTP server, are connected to the same local area network. We were able to achieve around 1 ms precision among the hosts and our NTP server,

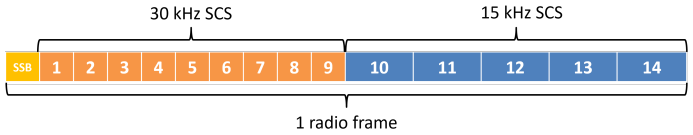

Fig. 3. The waveform structure; numbers denote slot numbers with different PDSCH configurations.

Table 1. Waveform slot PDSCH configurations [3]

Slot Number	MCS Index	Modulation	Target Code Rate x [1024]	Spectral Efficiency
1	0	QPSK	120	0.2344
2	5	QPSK	379	0.7402
3	9	QPSK	679	1.3262
4	11	16-QAM	378	1.4766
5	13	16-QAM	490	1.9141
6	16	16-QAM	658	2.5703
7	17	64-QAM	438	2.5664
8	19	64-QAM	517	3.0293
9	22	64-QAM	666	3.9023
10	0	QPSK	120	0.2344
11	9	QPSK	679	1.3262
12	11	16-QAM	378	1.4766
13	16	16-QAM	658	2.5703
14	17	64-QAM	438	2.5664

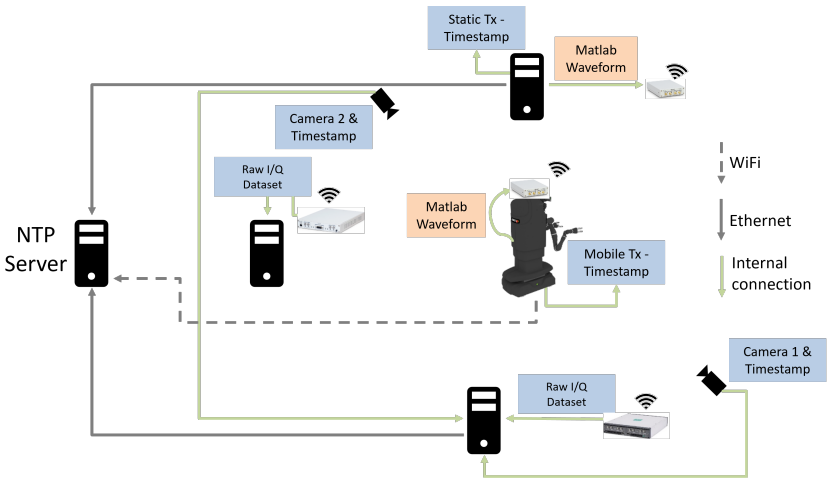

Fig. 4. Synchronization setup and data collection details.

which is similar to the observation in [55]. The connections for the synchronization setup along with the details of hosts' data collection are depicted in Fig. 4.

Measurement consists of 30 different runs, each taking around 3-4 minutes. The synchronization is corrected to *ms* precision before each measurement run. During each run, 30 radio transmissions per second are sent by transmitters, but static and mobile user transmissions are separated by 16.67 ms to prevent interference and ensure each of them is linked to a camera frame. In other words, considering the 60 fps operation, on each camera frame, there exists a transmission from one of the users. In order to increase the similarity between runs and ease the ML training, we have

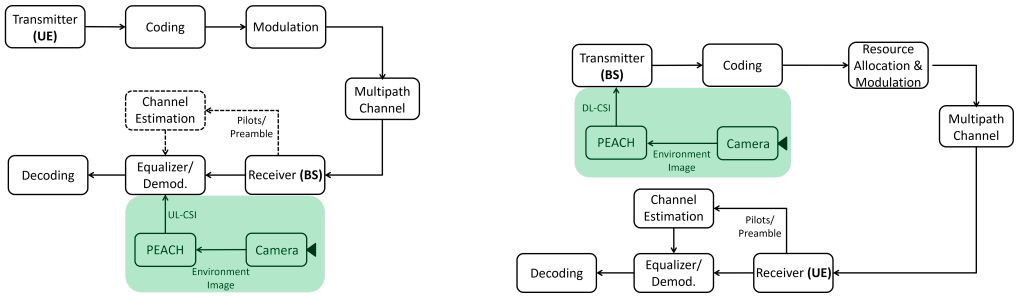

(a) PEACH system for UL (b) PEACH system for DL

Fig. 5. The OFDM communication system (simplified) with PEACH integrated.

used 15 different mobility patterns on the robot.[3] However, as explained in Section 3.2, there still exist differences due to the non-deterministic behaviour of the navigation execution. There is an additional measurement run for investigating the interference scenario, which is further explained in Section 5.3. The dataset consists of approximately 190, 000 raw I/Q transmissions stored in total per receiver from each transmitter. Therefore, for the dataset used in the CNN training we have around 190, 000 *CSI estimation-camera image pairs* in total per receiver and per transmitter.[4]

4 PEACH

In this section, first we provide a system overview of PEACH. Then, we describe how data are pre-processed. This is followed by the CNN architecture and the training process.

4.1 An Overview of PEACH

PEACH maps the depth images to the CSI amplitudes with the help of a CNN via supervised learning. By utilizing such visual environment information, PEACH provides environmental awareness to the RRM which allows proactive and intelligent algorithms to be employed without depending on feedback or pilot transmission. While being a novel contribution, PEACH can be integrated into existing 5G systems, in fact to any OFDM system, without the need to adjust to the standard in use. The proposed architecture for an integration to the OFDM systems is depicted in Fig. 5, where Fig. 5a and Fig. 5b illustrates UL and DL architecture, respectively.

Ensuring future CSI knowledge on base stations via our proposed architectures not only improves the latency, which is of paramount importance in URLLC, with reduction in processing and feedback delay and better CSI knowledge in interference scenarios (see Section 5.3) while not requiring metadata, but also enables RRM algorithms to be optimal [26, 45].

4.2 Data Pre-processing

In order to have faster training and real-time inference possibility, data pre-processing has been performed on the dataset before training. The applied pre-processing reduces the input sizes that yields less complex CNN architecture, which is of course less GPU-demanding.

The collected depth images from the cameras are in 720×1280 resolution. First, the images are cropped to size 700×800, to exclude including pixels the mobile robot never visits, and then they are downsampled to size 117×134, which is the final input size.

[3]Two consecutive runs use the same navigation plan on the robot.
[4]Since we assume block-fading during a radio frame, CSI estimations per SCS are the same throughout different slots for the same radio frame transmission.

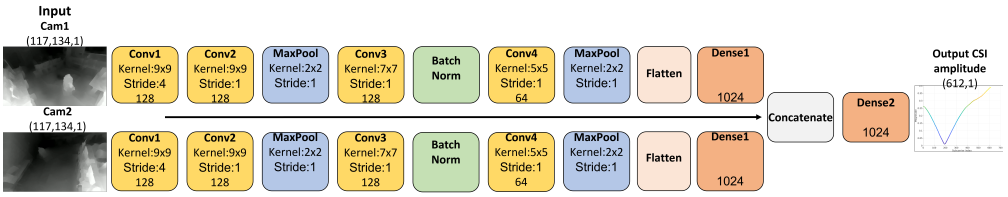

Fig. 6. The CNN architecture of PEACH.

The recorded raw I/Q datasets on each receiver are first analyzed to find starting transmission instances per transmitter per measurement run. Afterwards, CSI estimations of each transmission are parsed from the raw datasets with various estimation methods. The estimation methods used in dataset parsing are *DMRS-based pilot estimation* and its variants with fewer pilots, LS estimation[5] and *Full-Mean estimation*, which is the LS estimation averaged only over time for the entire waveform[6]. Later, the amplitude of the *Full-Mean estimation* is used as the output of the PEACH CNN architecture. The reason why PEACH is not trained for the CSI phase is explained in Section 6.2.

4.3 CNN Architecture and Training

The proposed PEACH CNN architecture is displayed in Fig. 6.[7] The details of each layer, such as the filter size of the convolutional layers (Conv) and the dimension of fully connected (Dense) layers, are provided at the bottom of the respective boxes.

We follow a multimodal approach in the PEACH CNN architecture such that two camera images can be utilized in one model simultaneously to prevent any camera view blockages, where the latter is common in one-camera approach [42]. The two branches of the architecture are symmetrical. Hence, the input-camera images from both cameras undergo the same CNN. The outputs of the last layers in each branch are then flattened and concatenated after a dense layer. Lastly, we have two following dense layers while the last being the output layer with size 612×1 for CSI amplitudes of 30 kHz SCS. An example of CSI amplitude is illustrated at the output of the model in Fig. 6.

CSI amplitudes on the output layer and the depth images on the input layer are normalized before training. The training code is based on Tensorflow 2.2.4 [5] and Keras [14]. Nadam optimizer [19] is used with mean square error (MSE) loss metric with initial learning rate of 0.00005. The model is trained for 50 epochs, which is observed to be sufficient for an appropriate learning performance. Nevertheless, to avoid any overfitting, weights of the epoch which has the best validation set performance are used for evaluation. The hyperparameters in our architecture are selected empirically. The dataset is separated into *training*, *validation*, and *test* sets, where 28 measurement run datasets are used for training, one for validation, and one measurement run dataset is used as test set.

The model is trained on an Nvidia DGX platform with Tesla V100 GPUs, where the training time of a model is approximately two hours. The average inference time per CSI amplitude prediction is around 1 ms over Nvidia Tesla V100 GPU. Running PEACH over a more modest Nvidia Quadro RTX 5000 GPU, or over high-end Intel Core i7-11700K CPU, or over more modest AMD Ryzen 7 PRO 4750U CPU, the average inference time increases to 8.8 ms, 20.3 ms and 35.6 ms, respectively. Finally, PEACH is tested in a Tensorflow serving capable edge-computing node with Quadro RTX 5000 GPU where average and maximum inference time are observed to be 9.3 ms and 15.3 ms,

[5]LS estimation is the ground truth among the estimation methods here as it uses every subcarrier on the entire waveform as pilots, and to avoid noise in the estimation performs sliding window averaging over time and frequency.
[6]The averaging is to evade noise in the estimation and to have one mean estimation per radio frame for each subcarrier.
[7]Note that the sample input images in Fig. 6 are not pre-processed for ease of understanding to human vision.

respectively. Considering the inference time even on low-end devices and 100 ms future prediction capability, PEACH can be confidently deployed in real-time critical systems.

5 PERFORMANCE EVALUATION

In this section, we evaluate the performance of PEACH for each transmitter-receiver pair by quantifying the results in terms of BER and compare them to the traditional DMRS-based channel estimation methods. The BER results are provided for all modulations types for both transmitters and for both current and 100 ms future CSI amplitude prediction of PEACH.[8] To further elaborate the advantages of PEACH, we demonstrate the performance under interference scenario. Finally, we provide an evaluation summary for completeness, since the performance of PEACH shows similar trends on both static and mobile Tx.

In all evaluations, we start comparing the BER results of QPSK modulation, which is the lowest order MCS that is robust in bad channel conditions. Further, 16-QAM and 64-QAM results are illustrated to elicit performance on different modulation orders. The adaptive modulation and coding (AMC) algorithms in RRM opts for more conservative MCSs in case of bad channel conditions to enhance reliability. We foresee that the merit of PEACH is to provide accurate performance on conservative MCSs while sensing the environment to pave the way for intelligent AMC algorithms in RRM to be implemented. PEACH is designed to obtain efficacy for all modulation orders in similar reliability performance while preserving the performance on lower order MCSs.

All comparisons are illustrated as box plots. On all the plots, the line shows the median and pentagram displays the mean; y-axis is in logarithmic scale visualizing BER. The box plots are obtained by the mean BER evaluation on each measurement run against respective estimation. In the evaluations, *Full-Mean*, explained in Section 4.2, is used as the baseline estimation for PEACH[9], *DMRS* is the traditional pilot-based estimation, *DMRS-Half* is displaying the results of using half of the actual DMRS, *DMRS-Quarter* denotes the results using quarter of the actual DMRS, *PEACH (Current)* are the results of PEACH system predicting CSI amplitudes for the current time instant, and lastly *PEACH (Future)* provides the results for using PEACH system to predict 100 ms future CSI amplitude. The variants of DMRS are used to demonstrate how the performance is affected by reducing the pilots further. The relation of the results are observed to be the same among different estimations when varying the coding rate but keeping the modulation unchanged. Therefore, for each modulation only one coding rate is selected for the plots.

It is worth mentioning that in order to ensure there is no overfitting with CNN, all the results for PEACH are obtained over test sets. Hence, for each measurement run result with PEACH, a new CNN is trained where the evaluated measurement run is used as a test set.

5.1 Performance of Static User

In Fig. 7, the performance in terms of BER is illustrated for static Tx with QPSK modulation. Please note that the lower order MCSs of QPSK for static Tx resulted in no errors for most of the measurement runs for all estimations, including PEACH. Since box plots are visualized in logarithmic scale, the low order MCS results containing mostly no errors in the sets are omitted for the remainder of the paper but rather provided in Appendix B in Fig. 19, for both Rx1 and Rx2[10]. The results demonstrate that PEACH is capable of providing reliability while the communication is using QPSK modulation, i.e., during worse channel conditions. Furthermore, PEACH attains the full potential when compared to *Full-Mean*.

[8]Note that for the reliability evaluations the CSI phase for PEACH estimations are obtained from the DMRS phase estimations.
[9]Since *Full-Mean* is the training data for PEACH, the latter is bounded by the results of *Full-Mean*.
[10]Note that for Rx1 the lowest MCS resulted in no error for all sets. Hence, the second lowest MCS result, which is MCS index:5, is provided.

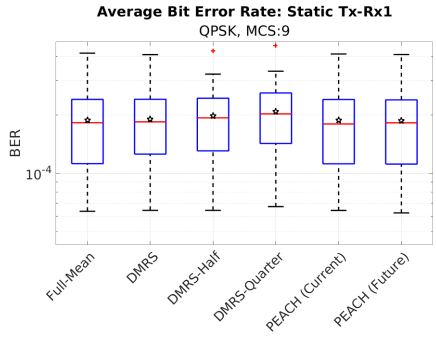

(a) Average BER: Static Tx-Rx1

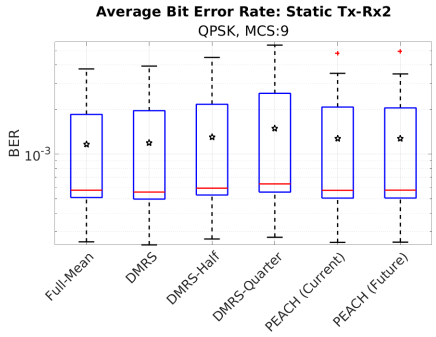

(b) Average BER: Static Tx-Rx2

Fig. 7. Average BER for static Tx with QPSK on both receivers.

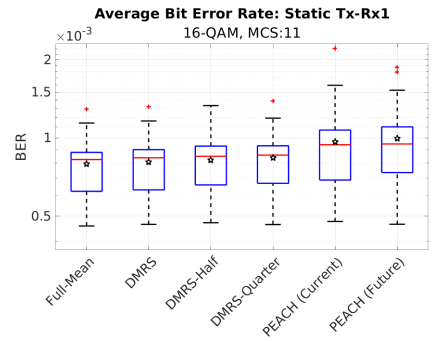

(a) Average BER: Static Tx-Rx1

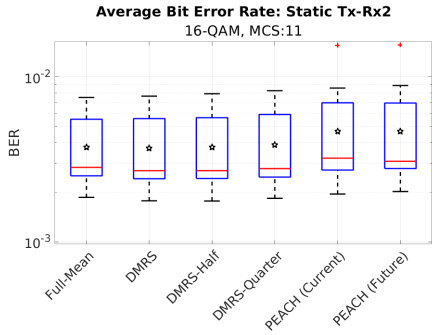

(b) Average BER: Static Tx-Rx2

Fig. 8. Average BER for static Tx with 16-QAM on both receivers.

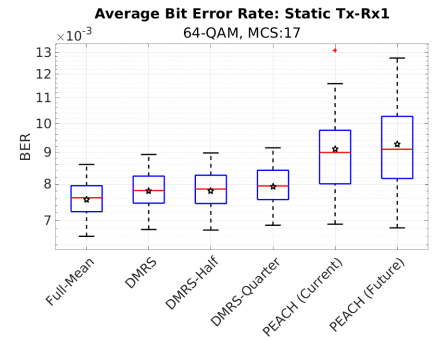

(a) Average BER: Static Tx-Rx1

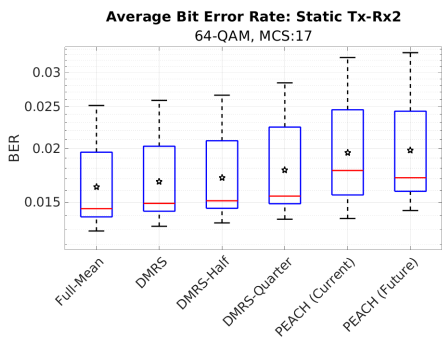

(b) Average BER: Static Tx-Rx2

Fig. 9. Average BER for static Tx with 64-QAM on both receivers.

Fig. 8 displays the BER performance of static Tx using 16-QAM. Although *DMRS* results are slightly better, PEACH performs similar on both receivers. Moreover, it is evident that for 16-QAM

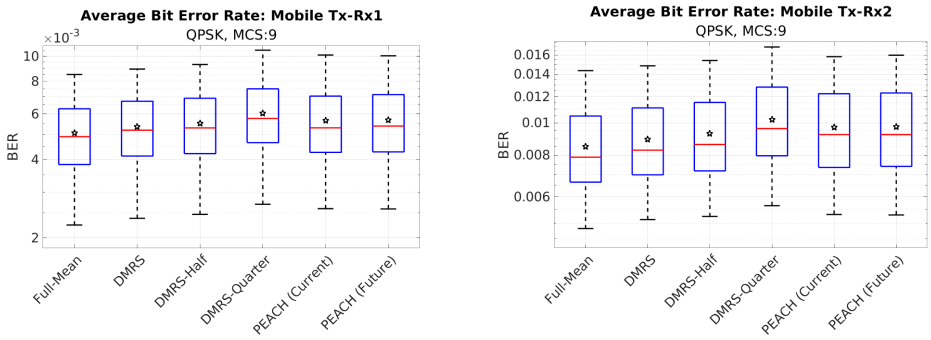

(a) Average BER: Mobile Tx-Rx1 (b) Average BER: Mobile Tx-Rx2

Fig. 10. Average BER for mobile Tx with QPSK on both receivers.

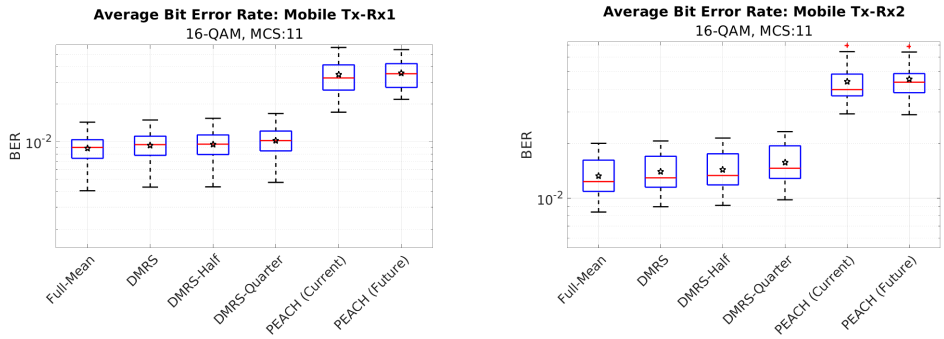

(a) Average BER: Mobile Tx-Rx1 (b) Average BER: Mobile Tx-Rx2

Fig. 11. Average BER for mobile Tx with 16-QAM on both receivers.

PEACH did not reach its full potential compared to *Full-Mean*. Therefore, further improving the CNN performance could potentially elevate the results of PEACH.

The BER performance of static Tx using 64-QAM on both receivers is visualized in Fig. 9. PEACH performance is reduced further in 64-QAM which depends more on accurate amplitude estimations. However, similar to the 16-QAM results, PEACH still has potential for further improvements.

5.2 Mobile User Performance

In Fig. 10, the BER performance is illustrated for mobile Tx with QPSK modulation. The results of mobile Tx case also demonstrate that PEACH is capable of providing reliability while the communication conditions are bad. Furthermore, PEACH reaches the full capacity similar to the static Tx when compared to *Full-Mean* for QPSK.

Fig. 11 displays the BER performance of mobile Tx using 16-QAM. *DMRS* results are notably better than PEACH for the mobile Tx for higher modulations. However, the performance gap between *Full-Mean* and PEACH indicates there is room for improvement similarly to the static Tx.

The BER performance when using 64-QAM on both receivers is shown in Fig. 12. PEACH's performance is similar to the 16-QAM case of mobile Tx.

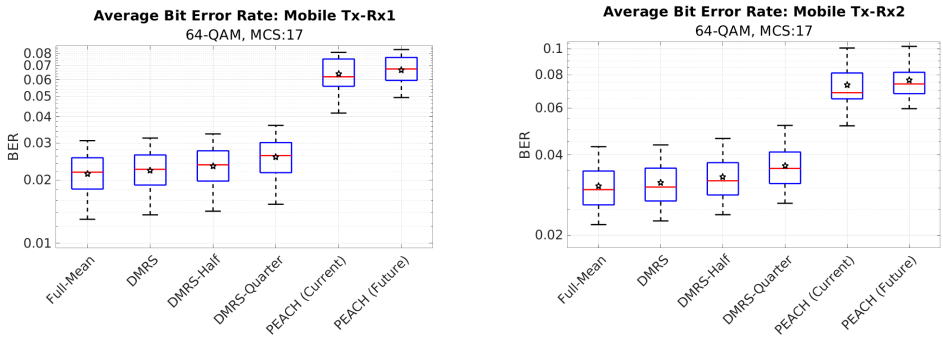

(a) Average BER: Mobile Tx-Rx1 (b) Average BER: Mobile Tx-Rx2

Fig. 12. Average BER for mobile Tx with 64-QAM on both receivers.

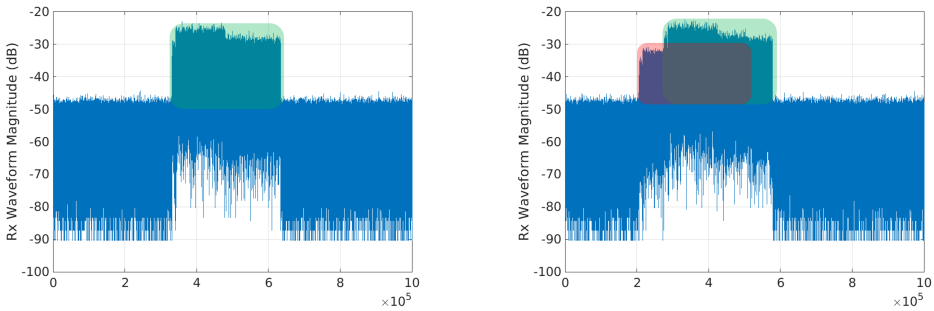

(a) (b)

Fig. 13. Waveforms of static Tx alone (a), interfering waveforms of static and mobile Tx (b).

5.3 Performance under Interference Scenario

The performance of pilot-based estimations is known to be severely influenced by interference [21]. In fact, jamming approaches targeting the pilots are observed to be more malicious [40]. Both are related with the fact that such cases prevent wireless channel estimations to obtain the actual fading channel. However, PEACH avoids such distortions by providing CSI even without reception. Therefore, we evaluated how PEACH could perform in a more realistic communication environment with interference scenario. In order to observe the system behavior in an interference scenario, we have an additional measurement run where all the transmissions are interfering. Only static Tx results are provided since for mobile Tx the interference is already quite strong for most of the transmissions. To facilitate the understanding of interference scenario, the static Tx waveform and the resulting interference waveform are provided in Fig. 13, where the x-axis denotes the samples in time and y-axis the waveform magnitude. Note that static Tx and mobile Tx are illustrated in transparent rectangular shapes in green and red colors, respectively.

The interference scenario comparisons are performed in terms of the Normalized Mean Square Error (NMSE), denoted by ε^2, and calculated as

$$\varepsilon^2 = \mathbb{E}\left[\frac{\|H_{LS} - H_{estimation}\|^2}{\|H_{estimation}\|^2}\right], \tag{2}$$

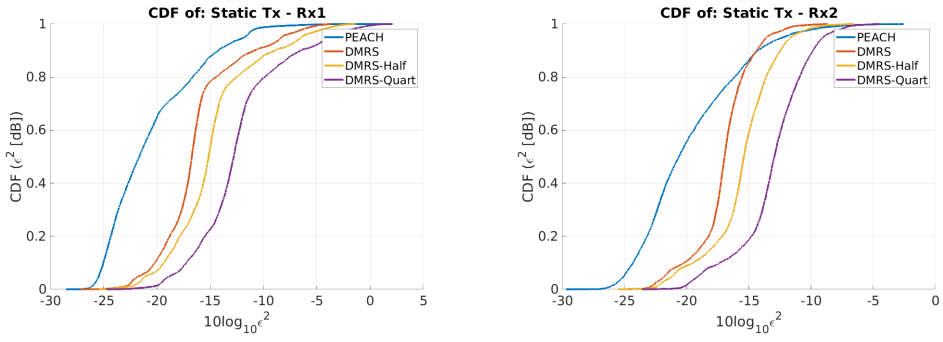

(a) (b)

Fig. 14. Empirical CDFs of NMSE per estimation method for Rx1 (a) and for Rx2 (b).

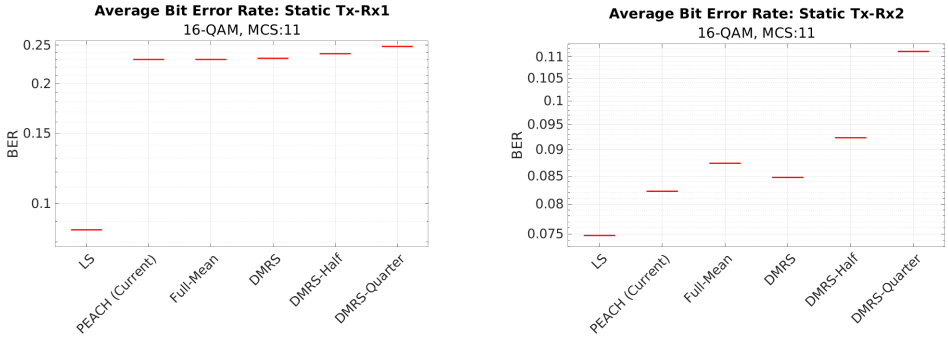

(a) (b)

Fig. 15. Average BER for static Tx with 16-QAM in interference scenario for Rx1 (a) and for Rx2 (b).

where H_{LS} is the ground truth and $H_{estimation}$ is the used estimation, either pilot- or PEACH-based, while performing the calculation. The resulting empirical cumulative distribution functions (CDFs) of ϵ^2 are visualized and compared in Fig. 14 in logarithmic scale for both receivers. PEACH improves the NMSE at the same empirical CDF up to 6 dB and 5 dB on Rx1 and Rx2, respectively. Since we have only one measurement run for the interference scenario, we provide the average BER over one set and display the mean of the entire set (with red line instead of pentagram for visual clarity) in Fig. 15 for both receivers. Since the BER among estimation methods reflects the same trend among all the modulations, only the 16-QAM results are displayed.

5.4 Evaluation Summary

The performance of PEACH is satisfactory with low modulation orders but gets worse in higher modulations for all transmitters. Yet, on all evaluations with higher modulations it is clear that PEACH is performing only slightly worse on both transmitters, with static Tx case being better. The difference can be explained with having higher variations on the CSI amplitudes of mobile Tx. We have observed that even slight movements of the robot result in significant changes in the CSI amplitude for the mobile Tx. Although omnidirectional antennas are used, due to non-idealities, the gains on all angles of the antenna are not equal. Hence, even a slight rotation or movement results in high variations on the CSI amplitude for the mobile Tx, while the static Tx is not affected

by that condition. Nonetheless, the deteriorated performance on higher modulations indicates that PEACH did not widely captured the CSI amplitude variations for several occasions although they are accurately addressed by *Full-Mean*. Therefore, it is worth noting that PEACH could be improved by ensuring better learning performance in the following ways: (1) Improving the CNN complexity by allowing higher resolution images to capture even slight movements; (2) Using recurrent neural network (RNN) models to leverage sequential information in consecutive images[11]; (3) Collecting more training data to avoid unseen movements, stemming from the non-deterministic movement of the robot and having multiple different mobility patterns.

An important evaluation note is on the results of Rx1 and Rx2 being similar for mobile Tx, while Rx2 performs worse for with the static Tx. The rationale behind this trend results from the static Tx facing straight towards Rx1 while the static Tx-Rx2 direction being from the side where antennas are observed to be performing worse. Yet, this phenomenon is not clearly observed on the mobile Tx as it is moving throughout the measurements, providing similar conditions to both receivers.

On a side note here, we would like to elaborate more on coherence time considerations in wireless communications. Considering our carrier frequency (3.74 GHz) and the maximum velocity of the robot, 0.15 m/s, the coherence time can be calculated to be approximately 0.5 s, using the coherence time formula [52]. Although CSI estimations from our measurements exhibit negligible variations in CSI amplitude during a radio frame, significant CSI variations are observed in almost all consecutive transmissions over a user which is separated by only $\sim$ 66.7 ms while moving.[12] In the light of these observations, it is worth noting that the coherence time limit assumptions with stochastic channel models would not hold for dynamic wireless conditions with non-idealities. Therefore, the practical conditions should be examined in a more intelligent manner especially for reliability and latency critical requirements such as URLLC. These results are compliant with the recent remarks on beyond 5G communications which are explained in Section 1. However, as long as in the environment there are not high speed movements resulting in abrupt changes within a camera frame (see Section 6.2), such an intelligent approach can be provided using PEACH.

6 DISCUSSION

In this section, we discuss potential use cases along with the encountered and foreseen limitations.

6.1 Potential Use Cases

Better CSI knowledge in non-ideal conditions. CSI corruption due to interference or noise can be vital for CSI parameter classification, which could degrade the overall system performance. CSI parameter classification in noisy environments is investigated in [65], where the authors performed CSI parameter classification with the help of CNNs with input being the received data. PEACH could provide such a classification without requiring to receive signal from user which avoids any noise or interference issue. Along with the considered UL improvements, PEACH avoids not only the feedback mechanism on DL but also the errors of CSI estimation on the user itself that could be affected by interference, jamming, erroneous or outdated estimation as well.

Proactive AMC algoritms. PEACH provides foresight and environmental awareness capability with similar reliability results compared to the traditional systems. Therefore, PEACH can pave the way towards implementation of proactive and intelligent AMC algorithms that could enable more securely aggressive MCS selections in advance. Such a novel AMC algorithm via PEACH could provide substantial gain with intelligent MCS selection where even better SNR-CQI mapping for

[11] Improving performance by using RNN was shown in [42]; however, in our evaluations we were not able to observe such gain and due to much higher training times, more trials on RNNs were left as future work.

[12] One reason for that is the non-idealities in the antenna, as explained in Section 5.4.

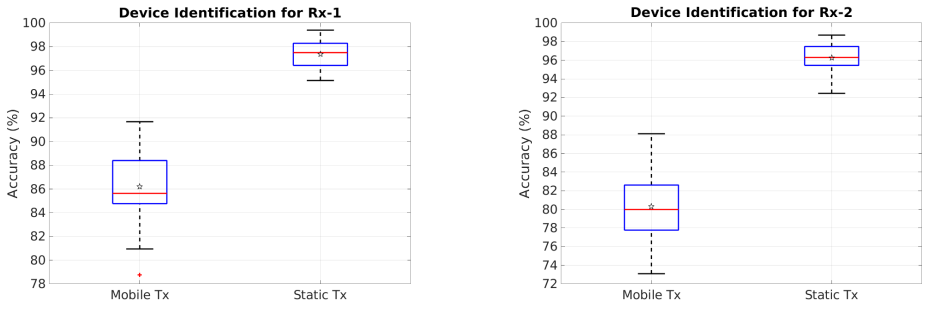

(a) (b)

Fig. 16. PEACH's device identification accuracy for Rx1 (a) and for Rx2 (b).

MCS selection is shown to provide improved network performance in terms of throughput gain up to 30% [62]. Using PEACH in AMC algorithms is deferred to future work.

Proactive resource allocation. Similar to the aforementioned proactive AMC algorithms, future channel knowledge of PEACH could be combined with resource allocation methods, such as [27], in order to allocate the wireless resources in a smarter way. Therefore, wireless resource allocation methods would use resource blocks more effectively for each user and avoid unnecessary channel uses in advance, which enhances the overall efficiency of wireless resource utilization.

Reliable GF access schemes. PEACH performed superior in the interference scenario which could enable base stations to mitigate from collision, interference or jamming cases. Providing solution to collision case in UL is vital in GF access schemes, especially for URLLC, where numerous collisions are expected at the base stations. PEACH could also make SIC practical in GF access schemes by providing the instantaneous CSI already in collision cases.

Impersonation attacks. CSI-based fingerprinting usage to detect devices or avoid impersonation attacks has gained attention recently [6, 66]. PEACH could provide potential enhancement for such use cases. Non-forgeable signature between user and base station, as discussed in [66], could be the instantaneous CSI between the communicating pairs which no attacker could imitate. User authentication based on CSI-based fingerprinting is already considered in literature but not with environmental awareness and not for mobile users [36]. For such a claim and extension, we have made an initial evaluation of PEACH's user/device identification potential, where PEACH decides which device transmitted the received message by comparing the estimated CSI amplitude to the predicted CSI amplitudes from PEACH for both static Tx and mobile Tx. The box plots illustrate the comparison results in Fig. 16 for both receivers performed over all measurement runs. Given that the average accuracy is around $96-97\%$ for static Tx and $80-86\%$ for mobile Tx for Rx2 and Rx1, it is clear that PEACH has the potential to be used in such a scenario with mobile users while providing high accuracy. However, it is required to be further tested with a higher number of users.

6.2 Limitations

CSI phase elusiveness. While parsing the dataset, we have observed that as long as the environment is the same, the CSI amplitudes are similar and useful to train the CNN. However, the CSI phases for the same environment are detected to be changing. The attempt to model the variations in CSI phases to make them useful for CNN training led to no success. Since we could not find an answer to model the variations, obtaining a mapping between images and CSI phases was not

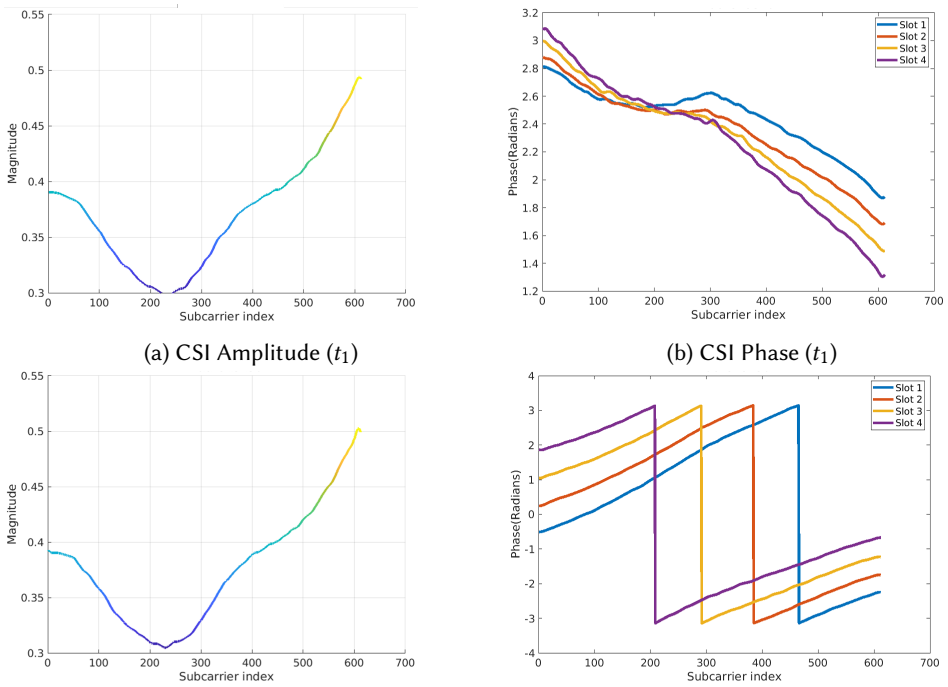

(a) CSI Amplitude (t_1)

(b) CSI Phase (t_1)

(c) CSI Amplitude (t_2)

(d) CSI Phase (t_2)

Fig. 17. CSI estimation amplitudes and phases for the same environment with time difference.

possible and is left for future work. The non-modeling phase issue is illustrated in Fig. 17, where t_1 and t_2 instances are separated by approximately 3 seconds and mobile Tx is being stationary for this period. If the phase issue is solved or modeled, it could potentially elevate PEACH further considering the results in Section 5.3, where high NMSE performance for CSI amplitudes did not clearly reflect on BER performance due to DMRS phase usage in decoding.

Camera limitations. Throughout this work, we have assumed a block-fading scenario over a radio frame which requires the coherence time to be larger than the radio frame (10 ms). However, for PEACH to operate reliably, the coherence time of the communication environment should be even higher, specifically above the camera frame interval which is $\frac{1}{\text{fps}} \approx 16.67$ ms for this work, such that we can assume a CSI amplitude per camera frame. Therefore, the performance of PEACH is limited to the frame rate of the camera, which should be able to capture the dynamic variations of the environment. Moreover, the ZED cameras used in our measurements utilize color images for depth perception instead of infrared sensors, which is observed to be performing worse in low-light conditions [64]. Thus, in case of environments with low-light conditions, PEACH could have potential problems if similar cameras were used.

Interference detection. Although PEACH provides better performance by avoiding the effects of interference, it cannot detect the interference occurrence. Unfortunately, this is a common drawback for all vision-wireless communications applications since there is no observation made on the radio. However, PEACH could be used to superposition DL transmissions with knowledge of actual CSI for the users from multiple base stations in order to reduce the effect of DL interference.

Unseen data case. The framework of PEACH depends on supervised training over data obtained from the considered environment. However, in case the geometry of the environment changes or a new mobility pattern is created which is entirely different compared to trained data, the performance of PEACH could deteriorate. Although PEACH is evaluated against test sets which are already unseen with varying mobility pattern, further testing is needed for PEACH when the geometry, devices, or environment change considerably.

Small movements. In order to reduce training and inference time, in our work the input images are downsampled by 6. Due to the resolution reduction, PEACH currently cannot capture the small rotation movements performed by the mobile robot (note that PEACH predictions change insignificantly for small rotation movements). As discussed in Section 5.4, employing recent RNN could potentially elicit better results by leveraging sequential information in images. However, we have observed long training times when using RNNs. Consequently, we defer their usage to future work.

A side note on limitations; with the advent of possible real-time ray-tracing in near future thanks to platforms such as Nvidia Sionna [24], real-time CSI acquisition would be realizable even for unseen environment changes by integrating these platforms within PEACH. Therefore, considering the real-time and proactive prediction possibility as well, our work provides potential to unravel the realization of foreseen digital twin based communication architectures towards wireless communication beyond 5G [28].

6.3 Capabilities of PEACH

Considering the results in Section 5, mobility has an impact on the performance of PEACH. Nevertheless, PEACH can cope with mobility successfully by reducing the modulation order, as illustrated in Fig. 10.

Considering the low modulation order results, PEACH is directly able to provide URLLC services for static users. For mobile users, BER results for lowest MCS indices are omitted for consistency between static user results. Nevertheless, these are provided in the Appendix B (Fig. 20). It is observed that PEACH attains even slightly better results compared to ground truth. However, the achieved results in BER (around 6×10^{-4}) are slightly below the range of URLLC services to be directly used. Nevertheless, these harsh channel conditions can be predicted by PEACH proactively via the 100 ms future prediction which can be combined with URLLC targeted resource allocation methods [27]. Along with such URLLC optimized resource allocation methods, the reliability range of PEACH can be enhanced to achieve values of reliability within the acceptance range for URLLC services for mobile users as well.

PEACH is built on CNN, considering the well known capability of capturing spatial information in 2D images. As mentioned in Section 5.4, PEACH could have leveraged sequential information in the videos by employing RNN, however, in our trials the training time increased considerably without improving the performance much. Hence, trials with RNN are left as future work.

The current CNN model used in PEACH is tested with two camera inputs but not limited to any number of input sources. In fact, in our trials we have observed better results with two camera inputs compared to single camera input. Nevertheless, since we still have $85 - 90$ ms advantage in time (left from the 100 ms future-prediction capability after the inference), even with the current system there is potential to scale it with more input sources.

The proof of concept is realized over two transmitters and two receivers. Since PEACH is trained separately for each transmitter-receiver pair, it can be used for more transmitter-receiver pairs. If we increase the number of pairs, the training time increases linearly. The inference time would be the same but computational resources needed at the edge node increase linearly with each additional transmitter-receiver pairs.

The use of PEACH is validated only for the indoor environment in the measurements. Nevertheless, it can be deployed in other environments as well. For each new environment another measurement campaign would be needed. The amount of data that would be sufficient for the intended operation is not analyzed in this work. Nevertheless, the performance variation depending on the amount of training data can be investigated with the released dataset in [10] for similar environments.

7 RELATED WORK

The related work corpus can be broadly classified into five categories, as described below.

7.1 Application of Computer Vision in Wireless Communications

Among the first applications of computer vision in the community of wireless communication is [42]. The system in [42] was proposed for mobility management in mmWave networks, specifically for making handover decisions. There was a single camera used in [42]. However, this led to the blind spot problem. To overcome that issue, in [30], the authors introduce two cameras. As a further improvement, the same authors in [31] use two cameras with 500 ms look-ahead capability for handovers in mmWave networks. Similarly, in [13], blockage prediction and beam prediction for mmWave networks is performed for multi user scenario but simulation-wise only. On a similar note, vision systems are used to predict the link quality, in terms of throughput, in 5.6 GHz WiFi systems [35]. They use object detection to predict the link throughput with 1 second look-ahead capability for an outdoor scenario which is in similar direction of the above mentioned works but in a 5.6 GHz WiFi system instead of mmWave. However, the decisions in these works are not based on CSI, which provides a more complete picture of the wireless channel conditions, but only on the received signal strength or on the visual detection of a blockage or on the observed link throughput. Another related work is [53], where a system called Argus is presented, which is capable of predicting the signal profile in mmWave communications from visual data. This in turn helps in finding the best picocell locations and yields maximum signal coverage. The most similar work to ours is [9], where a depth image based CNN architecture is used to predict the complex wireless channel impulse response. Although [9] provides more detailed information over the wireless channel, it was performed on 2.4 GHz in IEEE 802.15.4 with direct-sequence spread spectrum over 2 MHz bandwidth with only offset-QPSK modulation with one static transmitter and one receiver, and the information is transmitted in time domain. However, the adoption of OFDM systems is likely to be much greater while utilizing larger bandwidth and the information being transmitted in frequency-domain, where the estimation of channel state information in terms of channel frequency response is preferred.

Compared to the aforementioned works, we go a step beyond in PEACH by utilizing the CNN for predicting the current and 100 ms future CSI amplitudes in terms of channel frequency response over each subcarrier for OFDM systems, which is specifically tested in 5G NR for varying modulations over 20 MHz bandwidth.

7.2 Non-ideal Pilot or CQI Knowledge

While having perfect knowledge of channel conditions is very important for impeccable operation of wireless systems, this is very difficult to achieve. Hence, to bring the systems as close to a realistic behavior, different works make different assumptions which make the system behavior susceptible to deviations from perfect assumptions. For instance, in [21], the channel estimation is heavily affected by the interference. Further, sending/receiving outdated CQI leads to a poor performance [34]. The dynamic resource allocation process is especially vulnerable to non-timely

received CQI values. Therefore, in this work, by providing *timely* and *exact* CSI we could prevent the causes of severe performance degradation in wireless networks.

Another potential advantage of our approach could be in preventing jamming strategies. Namely, it was shown in [40] that jamming strategies that target directly pilots in OFDM systems outperform other jamming approaches. As our approach completely avoids pilots, we can prevent the additional harm coming from that type of jamming.

7.3 Metadata Reduction in OFDM Systems

The reduction of metadata in wireless communication is always one of the main targets while designing a new solution or even a new system, i.e., removal of the always on cell-reference signals in LTE systems on 5G NR. However, when considering the URLLC case, further reduction of metadata while not sacrificing the reliability is still challenging. For instance, as using too many pilots can be cumbersome, there were some efforts in performing channel estimation with reducing the number of pilot symbols. One such example is [39], with the focus on OFDM systems. However, while there is a reduction in the number of pilots, the performance is also sub-optimal as reduction is more emphasized. On the other hand, PEACH does not use pilots at all and still achieves a near-optimal performance compared to pilot-based techniques. Another approach to reduce metadata usage is presented in [23], where the channel quality indicator (CQI) feedback overhead can be reduced while guaranteeing the error rate. However, the proposed approach still includes overhead for CQI feedback and failing to estimate or report the CQI results in degradation, whereas in our work the CQI knowledge can be obtained via CSI amplitude and is always available through cameras without requiring reception of any feedback.

7.4 General ML Usage in Wireless Communications

Recently, there has been a significant usage of machine learning techniques in wireless communications. For instance, [63] and [54] tackle the problem of FDD reciprocity via deep learning to predict DL CSI knowledge using UL CSI. In [44], an end-to-end (E2E) learning of OFDM systems with general purpose was conducted, whereas in [7] the particular focus was the usage of E2E learning to reduce the pilot overhead in the OFDM system. Another ML-based related work is [67], where machine learning is used to extract channel estimation and for signal detection from received pilot symbols in an OFDM system. In [27], *experienced* deep reinforcement learning is used to provide model-free resource allocation for URLLC services where the transient training time problem of conventional deep reinforcement learning methods is avoided. However, aforementioned works were not tested in real measurements and no environment-related information was included in the respective systems, whereas both these concerns are addressed while providing a look-ahead capability (proactivity) with PEACH.

7.5 5G Datasets

As 5G are relatively new and still in the process of deployment (the first complete 5G network was put to work on April 2019), there are not many measurement data available, and especially not those that carry information on the indoor environment channel conditions. Most of the publicly-available datasets pertain to the pre-5G era, such as [61], which contain raw OFDM signals from LTE. A 5G-related dataset is presented in [51], which provides data only with KPIs such as CQI or bitrate. The most recent and closest dataset to our work is [8], where commercial data for the **n78 band**, collected in an outdoor-to-indoor setup, are provided, including those of power delay profile, the received power for each multipath. However, the dataset includes neither raw I/Q samples nor data obtained over SDRs. The dataset we are providing is on a baseband signal level, including the respective environment videos, with an overall size of around 3.4 TB [10]. Our dataset also allows

comparing performance of different MCS indices over real measurements since under block fading all slots (namely different MCS configurations in the waveform) are exposed to the same wireless channel. Such a dataset originates more potential for further research.

8 CONCLUSION

In this paper, we address the problem of accurately predicting 5G channel conditions in an OFDM-based wireless communication system, more exactly the URLLC types of service in dynamic environments. Our quantity of interest is CSI. In fundamental contrast to the state of the art, our machine learning based approach completely avoids the use of feedback and pilots. To that end, we built a system called PEACH, which uses environmental information with depth images, capable of accurately predicting CSI for the next 100 ms. We have experimentally validated our system through comprehensive measurements from an indoor environment, with two static receivers and two transmitters, where one of the latter was placed on top of a mobile robot. We showed that using environmental information a similar performance can be achieved as with pilot-based methods even without any radio metadata for both mobile and static users for multiple receivers. Furthermore, when interference-limited systems are considered, our approach can outperform the traditional methods by up to 6 dB in terms of NMSE. To the best of our knowledge, this is the first work demonstrating current and proactive per subcarrier CSI amplitude prediction with only environment images for multiple receivers and transmitters, including a mobile transmitter. Along the proposed novelty, our work provides also the first 5G dataset with raw I/Q signals obtained over multiple SDRs, including mobility. As part of the future work, we plan to build a system capable of predicting directly the value of CQI without any feedback from the user, by just using the environmental information. Another research direction we are planning to pursue is the investigation of providing intelligence and proactive capability to adaptive modulation and coding algorithms with the PEACH system.

ACKNOWLEDGEMENTS

This work has received funding from the Bavarian Ministry of Economic Affairs, Regional Development and Energy as part of the project ‘5G Testbed Bayern mit Schwerpunktanwendung eHealth’. The authors acknowledge the financial support by the Federal Ministry of Education and Research of Germany (BMBF) in the programme of "Souverän. Digital. Vernetzt." joint project 6G-life, project identification number 16KISK002.

REFERENCES

[1] 3GPP. 2017. *Study on Scenarios and Requirements for Next Generation Access Technologies.* Technical Specification (TS) 38.913. 3rd Generation Partnership Project (3GPP). Release 14.

[2] 3GPP. 2019. *Study on Physical Layer Enhancements for NR URLLC.* Technical Report (TR) 38.824. 3rd Generation Partnership Project (3GPP). Release 16.

[3] 3GPP. 2021. *Physical Layer Procedures for Data.* Technical Specification (TS) 38.214. 3rd Generation Partnership Project (3GPP). Release 16.

[4] 3GPP. 2022. *NR; Physical Channels and Modulation.* Technical Specification (TS) 38.211. 3rd Generation Partnership Project (3GPP). Release 16.

[5] Martín Abadi, Paul Barham, Jianmin Chen, Zhifeng Chen, Andy Davis, Jeffrey Dean, Matthieu Devin, Sanjay Ghemawat, Geoffrey Irving, Michael Isard, Manjunath Kudlur, Josh Levenberg, Rajat Monga, Sherry Moore, Derek G. Murray, Benoit Steiner, Paul Tucker, Vijay Vasudevan, Pete Warden, Martin Wicke, Yuan Yu, and Xiaoqiang Zheng. 2016. TensorFlow: A System for Large-Scale Machine Learning. In *Proceedings of the 12th USENIX Conference on Operating Systems Design and Implementation* (Savannah, GA, USA) *(OSDI'16)*. USENIX Association, USA, 265–283.

[6] Luis Fernando Abanto-Leon, Andreas Bäuml, Gek Hong (Allyson) Sim, Matthias Hollick, and Arash Asadi. 2020. Stay Connected, Leave No Trace: Enhancing Security and Privacy in WiFi via Obfuscating Radiometric Fingerprints. *Proc. ACM Meas. Anal. Comput. Syst.* 4, 3, Article 44 (nov 2020), 31 pages. https://doi.org/10.1145/3428329

[7] Fayçal Ait Aoudia and Jakob Hoydis. 2022. End-to-End Learning for OFDM: From Neural Receivers to Pilotless Communication. *IEEE Transactions on Wireless Communications* 21, 2 (2022), 1049–1063. https://doi.org/10.1109/TWC.2021.3101364

[8] Usman Ali, Giuseppe Caso, Luca De Nardis, Konstantinos Kousias, Mohammad Rajiullah, Özgü Alay, Marco Neri, Anna Brunstrom, and Maria-Gabriella Di Benedetto. 2022. Large-Scale Dataset for the Analysis of Outdoor-to-Indoor Propagation for 5G Mid-Band Operational Networks. *Data* 7, 3 (2022). https://doi.org/10.3390/data7030034

[9] Serkut Ayvaşık, H. Murat Gürsu, and Wolfgang Kellerer. 2019. Veni Vidi Dixi: Reliable Wireless Communication with Depth Images. In *Proceedings of the 15th International Conference on Emerging Networking Experiments And Technologies* (Orlando, Florida) *(CoNEXT '19)*. Association for Computing Machinery, New York, NY, USA, 172–185. https://doi.org/10.1145/3359989.3365418

[10] Serkut Ayvasik, Fidan Mehmeti, Edwin Babaians, and Wolfgang Kellerer. 2023. PEACH Proactive and Environment Aware Channel State Information Prediction with Depth Images - Dataset. https://doi.org/10.14459/2022mp1694552

[11] Ettus Knowledge Base. 2020. UHD — Ettus Knowledge Base. https://kb.ettus.com/index.php?title=UHD&oldid=4720 [Online; accessed 10-October-2022].

[12] Emil Björnson, Luca Sanguinetti, Henk Wymeersch, Jakob Hoydis, and Thomas L. Marzetta. 2019. Massive MIMO is a reality—What is next?: Five promising research directions for antenna arrays. *Digital Signal Processing* 94 (2019), 3–20. https://doi.org/10.1016/j.dsp.2019.06.007 Special Issue on Source Localization in Massive MIMO.

[13] Gouranga Charan, Muhammad Alrabeiah, and Ahmed Alkhateeb. 2021. Vision-Aided 6G Wireless Communications: Blockage Prediction and Proactive Handoff. *IEEE Transactions on Vehicular Technology* 70, 10 (2021), 10193–10208. https://doi.org/10.1109/TVT.2021.3104219

[14] François Chollet et al. 2015. Keras. https://keras.io.

[15] S. Coleri, M. Ergen, A. Puri, and A. Bahai. 2002. Channel estimation techniques based on pilot arrangement in OFDM systems. *IEEE Transactions on Broadcasting* 48, 3 (2002), 223–229. https://doi.org/10.1109/TBC.2002.804034

[16] Shi-Gang Cui, Hui Wang, and Li Yang. 2012. A simulation study of A-star algorithm for robot path planning. In *16th international conference on mechatronics technology*. 506–510.

[17] Tiago P.C. De Andrade, Carlos A. Astudillo, Luiz R. Sekijima, and Nelson L.S. Da Fonseca. 2017. The Random Access Procedure in Long Term Evolution Networks for the Internet of Things. *IEEE Communications Magazine* 55, 3 (2017), 124–131. https://doi.org/10.1109/MCOM.2017.1600555CM

[18] Jie Ding, Mahyar Nemati, Shiva Raj Pokhrel, Ok-Sun Park, Jinho Choi, and Fumiyuki Adachi. 2022. Enabling Grant-Free URLLC: An Overview of Principle and Enhancements by Massive MIMO. *IEEE Internet of Things Journal* 9, 1 (2022), 384–400. https://doi.org/10.1109/JIOT.2021.3107242

[19] Timothy Dozat. 2016. Incorporating nesterov momentum into adam. (2016).

[20] Giuseppe Durisi, Tobias Koch, and Petar Popovski. 2016. Toward Massive, Ultrareliable, and Low-Latency Wireless Communication With Short Packets. *Proc. IEEE* 104, 9 (2016), 1711–1726. https://doi.org/10.1109/JPROC.2016.2537298

[21] Ulrich Epple and Michael Schnell. 2010. Channel Estimation in OFDM Systems with Strong Interference. (2010).

[22] Gerhard P. Fettweis. 2014. The Tactile Internet: Applications and Challenges. *IEEE Vehicular Technology Magazine* 9, 1 (2014), 64–70. https://doi.org/10.1109/MVT.2013.2295069

[23] Samira Homayouni, Stefan Schwarz, Martin Klaus Mueller, and Markus Rupp. 2018. CQI mapping optimization in spatial wireless channel prediction. In *2018 IEEE 87th Vehicular Technology Conference (VTC Spring)*. IEEE, 1–5.

[24] Jakob Hoydis, Sebastian Cammerer, Fayçal Ait Aoudia, Avinash Vem, Nikolaus Binder, Guillermo Marcus, and Alexander Keller. 2022. Sionna: An Open-Source Library for Next-Generation Physical Layer Research. *arXiv preprint* (Mar. 2022).

[25] Hyoungju Ji, Sunho Park, Jeongho Yeo, Younsun Kim, Juho Lee, and Byonghyo Shim. 2018. Ultra-Reliable and Low-Latency Communications in 5G Downlink: Physical Layer Aspects. *IEEE Wireless Communications* 25, 3 (2018), 124–130. https://doi.org/10.1109/MWC.2018.1700294

[26] Igor Kadota, Muhammad Shahir Rahman, and Eytan Modiano. 2021. WiFresh: Age-of-Information from Theory to Implementation. In *2021 International Conference on Computer Communications and Networks (ICCCN)*. 1–11. https://doi.org/10.1109/ICCCN52240.2021.9522228

[27] Ali Taleb Zadeh Kasgari, Walid Saad, Mohammad Mozaffari, and H. Vincent Poor. 2021. Experienced Deep Reinforcement Learning With Generative Adversarial Networks (GANs) for Model-Free Ultra Reliable Low Latency Communication. *IEEE Transactions on Communications* 69, 2 (2021), 884–899. https://doi.org/10.1109/TCOMM.2020.3031930

[28] Latif U. Khan, Walid Saad, Dusit Niyato, Zhu Han, and Choong Seon Hong. 2022. Digital-Twin-Enabled 6G: Vision, Architectural Trends, and Future Directions. *IEEE Communications Magazine* 60, 1 (2022), 74–80. https://doi.org/10.1109/MCOM.001.21143

[29] Kwang Soon Kim, Dong Ku Kim, Chan-Byoung Chae, Sunghyun Choi, Young-Chai Ko, Jonghyun Kim, Yeon-Geun Lim, Minho Yang, Sundo Kim, Byungju Lim, Kwanghoon Lee, and Kyung Lin Ryu. 2019. Ultrareliable and Low-Latency Communication Techniques for Tactile Internet Services. *Proc. IEEE* 107, 2 (2019), 376–393. https://doi.org/10.1109/

JPROC.2018.2868995

[30] Yusuke Koda, Kota Nakashima, Koji Yamamoto, Takayuki Nishio, and Masahiro Morikura. 2020. Cooperative Sensing in Deep RL-Based Image-to-Decision Proactive Handover for mmWave Networks. In *2020 IEEE 17th Annual Consumer Communications and Networking Conference (CCNC)*. 1–6. https://doi.org/10.1109/CCNC46108.2020.9045186

[31] Yusuke Koda, Kota Nakashima, Koji Yamamoto, Takayuki Nishio, and Masahiro Morikura. 2020. Handover Management for mmWave Networks With Proactive Performance Prediction Using Camera Images and Deep Reinforcement Learning. *IEEE Transactions on Cognitive Communications and Networking* 6, 2 (2020), 802–816. https://doi.org/10.1109/TCCN.2019.2961655

[32] Stefan Kohlbrecher, Johannes Meyer, Thorsten Graber, Karen Petersen, Uwe Klingauf, and Oskar von Stryk. 2013. Hector open source modules for autonomous mapping and navigation with rescue robots. In *Robot Soccer World Cup*. Springer, 624–631.

[33] Stefan Kohlbrecher, Oskar Von Stryk, Johannes Meyer, and Uwe Klingauf. 2011. A flexible and scalable SLAM system with full 3D motion estimation. In *2011 IEEE international symposium on safety, security, and rescue robotics*. IEEE, 155–160.

[34] A. S. Konstantinov and A. V. Pestryakov. 2019. Fading Channel Prediction for 5G. In *2019 Systems of Signal Synchronization, Generating and Processing in Telecommunications (SYNCHROINFO)*. 1–7. https://doi.org/10.1109/SYNCHROINFO.2019.8813950

[35] Riichi Kudo, Kahoko Takahashi, Takeru Inoue, and Kohei Mizuno. 2020. Using Vision-Based Object Detection for Link Quality Prediction in 5.6-GHz Channel. *EURASIP J. Wirel. Commun. Netw.* 2020, 1 (oct 2020), 21 pages. https://doi.org/10.1186/s13638-020-01829-8

[36] Hongbo Liu, Yan Wang, Jian Liu, Jie Yang, and Yingying Chen. 2014. Practical User Authentication Leveraging Channel State Information (CSI). In *Proceedings of the 9th ACM Symposium on Information, Computer and Communications Security* (Kyoto, Japan) *(ASIA CCS '14)*. Association for Computing Machinery, New York, NY, USA, 389–400. https://doi.org/10.1145/2590296.2590321

[37] Zhenyu Liu, Lin Zhang, and Zhi Ding. 2019. Exploiting Bi-Directional Channel Reciprocity in Deep Learning for Low Rate Massive MIMO CSI Feedback. *IEEE Wireless Communications Letters* 8, 3 (2019), 889–892. https://doi.org/10.1109/LWC.2019.2898662

[38] Nurul Huda Mahmood, Renato Abreu, Ronald Böhnke, Martin Schubert, Gilberto Berardinelli, and Thomas H. Jacobsen. 2019. Uplink Grant-Free Access Solutions for URLLC services in 5G New Radio. In *2019 16th International Symposium on Wireless Communication Systems (ISWCS)*. 607–612. https://doi.org/10.1109/ISWCS.2019.8877253

[39] Mahdi Boloursaz Mashhadi and Deniz Gündüz. 2021. Pruning the Pilots: Deep Learning-Based Pilot Design and Channel Estimation for MIMO-OFDM Systems. *IEEE Transactions on Wireless Communications* 20, 10 (2021), 6315–6328. https://doi.org/10.1109/TWC.2021.3073309

[40] Daniel M. Mielke, Thomas Gräupl, and Ayten Gürbüz. 2021. Impact of Pilot Jamming Attacks on Digital Aeronautical Data Communications. In *2021 IEEE/AIAA 40th Digital Avionics Systems Conference (DASC)*. 1–10. https://doi.org/10.1109/DASC52595.2021.9594335

[41] Takayuki Nishio, Yusuke Koda, Jihong Park, Mehdi Bennis, and Klaus Doppler. 2021. When Wireless Communications Meet Computer Vision in Beyond 5G. *IEEE Communications Standards Magazine* 5, 2 (2021), 76–83. https://doi.org/10.1109/MCOMSTD.001.2000047

[42] Takayuki Nishio, Hironao Okamoto, Kota Nakashima, Yusuke Koda, Koji Yamamoto, Masahiro Morikura, Yusuke Asai, and Ryo Miyatake. 2019. Proactive Received Power Prediction Using Machine Learning and Depth Images for mmWave Networks. *IEEE Journal on Selected Areas in Communications* 37, 11 (2019), 2413–2427. https://doi.org/10.1109/JSAC.2019.2933763

[43] Mehmet Kemal Ozdemir and Huseyin Arslan. 2007. Channel estimation for wireless ofdm systems. *IEEE Communications Surveys and Tutorials* 9, 2 (2007), 18–48. https://doi.org/10.1109/COMST.2007.382406

[44] Timothy O'Shea and Jakob Hoydis. 2017. An Introduction to Deep Learning for the Physical Layer. *IEEE Transactions on Cognitive Communications and Networking* 3, 4 (2017), 563–575. https://doi.org/10.1109/TCCN.2017.2758370

[45] Arled Papa, Polina Kutsevol, Fidan Mehmeti, and Wolfgang Kellerer. 2022. Effects of SD-RAN Control Plane Design on User Quality of Service. In *2022 IEEE 8th International Conference on Network Softwarization (NetSoft)*. 312–320. https://doi.org/10.1109/NetSoft54395.2022.9844029

[46] Jihong Park, Sumudu Samarakoon, Hamid Shiri, Mohamed K Abdel-Aziz, Takayuki Nishio, Anis Elgabli, and Mehdi Bennis. 2022. Extreme ultra-reliable and low-latency communication. *Nature Electronics* 5, 3 (2022), 133–141.

[47] Klaus I. Pedersen, Gilberto Berardinelli, Frank Frederiksen, Preben Mogensen, and Agnieszka Szufarska. 2016. A flexible 5G frame structure design for frequency-division duplex cases. *IEEE Communications Magazine* 54, 3 (2016), 53–59. https://doi.org/10.1109/MCOM.2016.7432148

[48] Guillermo Pocovi, Hamidreza Shariatmadari, Gilberto Berardinelli, Klaus Pedersen, Jens Steiner, and Zexian Li. 2018. Achieving Ultra-Reliable Low-Latency Communications: Challenges and Envisioned System Enhancements. *IEEE*

Network 32, 2 (2018), 8–15. https://doi.org/10.1109/MNET.2018.1700257

[49] Nicolas Pontois, Megumi Kaneko, Thi Ha Ly Dinh, and Lila Boukhatem. 2018. User Pre-Scheduling and Beamforming with Outdated CSI in 5G Fog Radio Access Networks. In *2018 IEEE Global Communications Conference (GLOBECOM)*. 1–6. https://doi.org/10.1109/GLOCOM.2018.8647539

[50] Petar Popovski, Kasper Fløe Trillingsgaard, Osvaldo Simeone, and Giuseppe Durisi. 2018. 5G Wireless Network Slicing for eMBB, URLLC, and mMTC: A Communication-Theoretic View. *IEEE Access* 6 (2018), 55765–55779. https://doi.org/10.1109/ACCESS.2018.2872781

[51] Darijo Raca, Dylan Leahy, Cormac J. Sreenan, and Jason J. Quinlan. 2020. Beyond Throughput, the next Generation: A 5G Dataset with Channel and Context Metrics. In *Proceedings of the 11th ACM Multimedia Systems Conference* (Istanbul, Turkey) *(MMSys '20)*. Association for Computing Machinery, New York, NY, USA, 303–308. https://doi.org/10.1145/3339825.3394938

[52] Theodore S Rappaport et al. 1996. *Wireless communications: principles and practice*. Vol. 2. prentice hall PTR New Jersey.

[53] Hem Regmi and Sanjib Sur. 2022. Argus: Predictable Millimeter-Wave Picocells with Vision and Learning Augmentation. *Proc. ACM Meas. Anal. Comput. Syst.* 6, 1, Article 2 (feb 2022), 26 pages. https://doi.org/10.1145/3508022

[54] Mohammad Sadegh Safari, Vahid Pourahmadi, and Shabnam Sodagari. 2020. Deep UL2DL: Data-Driven Channel Knowledge Transfer From Uplink to Downlink. *IEEE Open Journal of Vehicular Technology* 1 (2020), 29–44. https://doi.org/10.1109/OJVT.2019.2962631

[55] Sandeep Singh Sandha, Joseph Noor, Fatima M. Anwar, and Mani Srivastava. 2019. Exploiting Smartphone Peripherals for Precise Time Synchronization. In *2019 IEEE Global Conference on Signal and Information Processing (GlobalSIP)*. 1–6. https://doi.org/10.1109/GlobalSIP45357.2019.8969519

[56] Changyang She, Chengjian Sun, Zhouyou Gu, Yonghui Li, Chenyang Yang, H. Vincent Poor, and Branka Vucetic. 2021. A Tutorial on Ultrareliable and Low-Latency Communications in 6G: Integrating Domain Knowledge Into Deep Learning. *Proc. IEEE* 109, 3 (2021), 204–246. https://doi.org/10.1109/JPROC.2021.3053601

[57] Changyang She, Chenyang Yang, and Tony Q. S. Quek. 2017. Radio Resource Management for Ultra-Reliable and Low-Latency Communications. *IEEE Communications Magazine* 55, 6 (2017), 72–78. https://doi.org/10.1109/MCOM.2017.1601092

[58] Meryem Simsek, Adnan Aijaz, Mischa Dohler, Joachim Sachs, and Gerhard Fettweis. 2016. 5G-Enabled Tactile Internet. *IEEE Journal on Selected Areas in Communications* 34, 3 (2016), 460–473. https://doi.org/10.1109/JSAC.2016.2525398

[59] Christoph Sprunk, Boris Lau, Patrick Pfaff, and Wolfram Burgard. 2017. An accurate and efficient navigation system for omnidirectional robots in industrial environments. *Autonomous Robots* 41, 2 (2017), 473–493.

[60] Stereolabs. 2022. ZED SDK. https://github.com/stereolabs/zed-examples [Online; accessed 10-October-2022].

[61] Kürşat Tekbiyik, Özkan Akbunar, Ali Rıza Ekti, Ali Görçin, and Güneş Karabulut Kurt. 2020. COSINE: Cellular cOmmunication SIgNal datasEt. https://doi.org/10.21227/SAFR-GH59

[62] Abitha K Thyagarajan, Priyeash Balasubramanian, Vydeki D, and Karthik M. 2021. SNR-CQI Mapping for 5G Downlink Network. In *2021 IEEE Asia Pacific Conference on Wireless and Mobile (APWiMob)*. 173–177. https://doi.org/10.1109/APWiMob51111.2021.9435258

[63] Wolfgang Utschick, Valentina Rizzello, Michael Joham, Zhengxiang Ma, and Leonard Piazzi. 2022. Learning the CSI Recovery in FDD Systems. *IEEE Transactions on Wireless Communications* 21, 8 (2022), 6495–6507. https://doi.org/10.1109/TWC.2022.3149946

[64] V S K P Varma, S Adarsh, K I Ramachandran, and Binoy B Nair. 2018. Real Time Detection of Speed Hump/Bump and Distance Estimation with Deep Learning using GPU and ZED Stereo Camera. *Procedia Computer Science* 143 (2018), 988–997. https://doi.org/10.1016/j.procs.2018.10.335 8th International Conference on Advances in Computing and Communications (ICACC-2018).

[65] Ankur Vora, Pierre-Xavier Thomas, Rong Chen, and Kyoung-Don Kang. 2019. CSI Classification for 5G via Deep Learning. In *2019 IEEE 90th Vehicular Technology Conference (VTC2019-Fall)*. 1–5. https://doi.org/10.1109/VTCFall.2019.8891133

[66] Qiang Xu, Rong Zheng, Walid Saad, and Zhu Han. 2016. Device Fingerprinting in Wireless Networks: Challenges and Opportunities. *IEEE Communications Surveys and Tutorials* 18, 1 (2016), 94–104. https://doi.org/10.1109/COMST.2015.2476338

[67] Hao Ye, Geoffrey Ye Li, and Biing-Hwang Juang. 2018. Power of Deep Learning for Channel Estimation and Signal Detection in OFDM Systems. *IEEE Wireless Communications Letters* 7, 1 (2018), 114–117. https://doi.org/10.1109/LWC.2017.2757490

[68] Kaiyu Zheng. 2021. Ros navigation tuning guide. In *Robot Operating System (ROS)*. Springer, 197–226.

A VISUALIZATION OF NON-DETERMINISTIC ROBOT MOBILITY

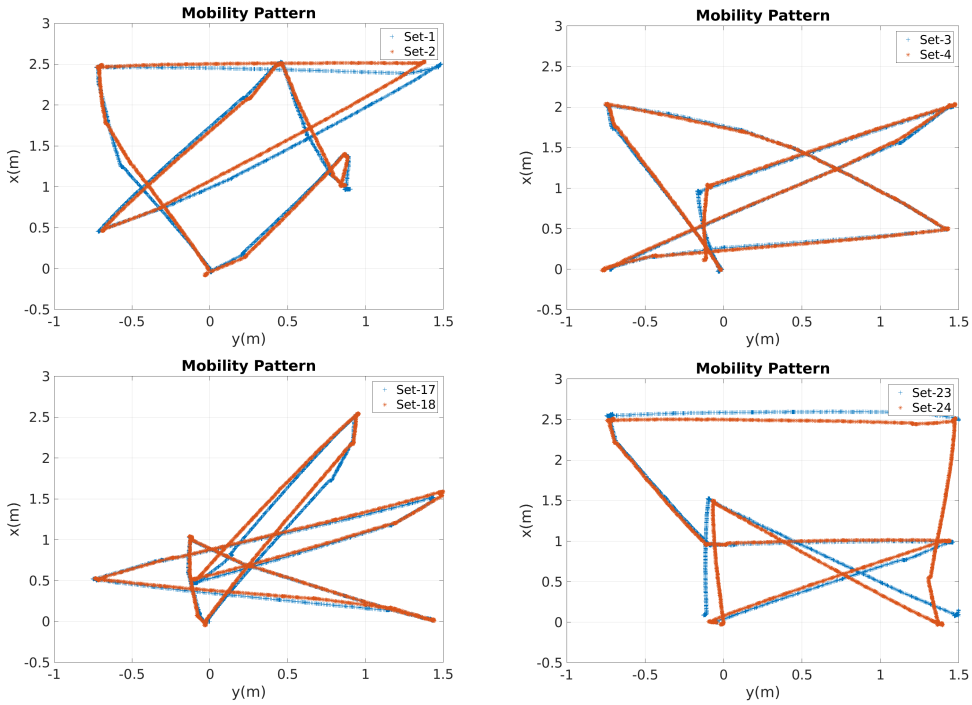

Fig. 18. Deviation of mobile robot location in consecutive measurement runs.

B LOW MODULATION ORDER RESULTS

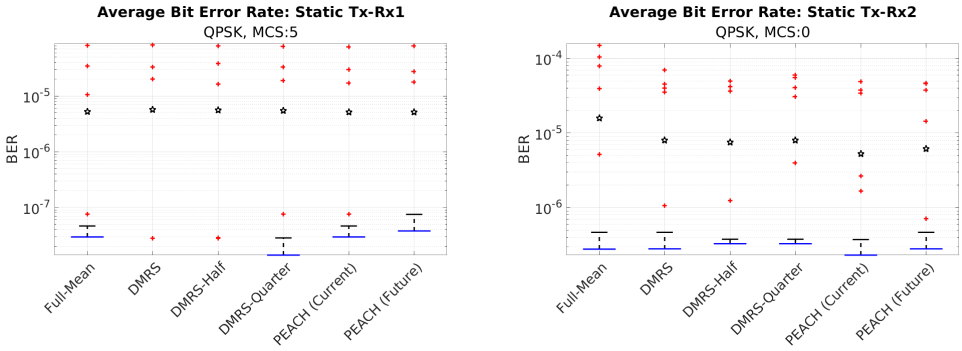

(a) Average BER: Static Tx-Rx1

(b) Average BER: Static Tx-Rx2

Fig. 19. Average BER for static Tx with QPSK on both receivers for low MCS indices.

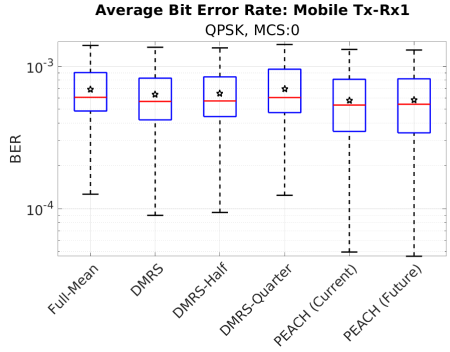

(a) Average BER: Mobile Tx-Rx1

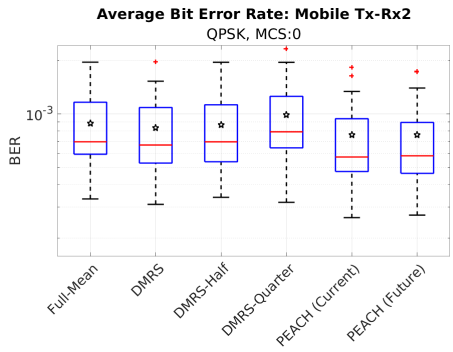

(b) Average BER: Mobile Tx-Rx2

Fig. 20. Average BER for mobile Tx with QPSK on both receivers for low MCS indices.

Received October 2022; revised December 2022; accepted January 2023